Energy Storage Materials 20 (2019) 470

Contents lists available at ScienceDirect

Energy Storage Materials

journal homepage: www.elsevier.com/locate/ensm

Corrigendum

Corrigendum to "Moderately concentrated electrolyte improves solid–electrolyte interphase and sodium storage performance of hard carbon" Energy Storage Mater. 16 (2019) 146–154

Jagabandhu Patra[a,d], Hao-Tzu Huang[a], Weijiang Xue[b], Chao Wang[b,c], Ahmed S. Helal[b], Ju Li[b], Jeng-Kuei Chang[a,b,d]

[a] *Institute of Materials Science and Engineering, National Central University, Taoyuan, Taiwan, ROC*
[b] *Department of Nuclear Science and Engineering and Department of Materials Science and Engineering, Massachusetts Institute of Technology, Cambridge, USA*
[c] *School of Materials Science and Engineering, Tongji University, Shanghai 201804, China*
[d] *Hierarchical Green-Energy Materials (Hi-GEM) Research Center, National Cheng Kung University, Tainan, Taiwan, ROC*

The authors regret to modify the author affiliations.

The authors would like to apologise for any inconvenience caused.

DOI of original article: http://dx.doi.org/10.1016/j.ensm.2018.04.022
E-mail address: jkchang@nctu.edu.tw (J.-K. Chang).

https://doi.org/10.1016/j.ensm.2019.02.008

Available online 13 February 2019

Energy Storage Materials 16 (2019) 146–154

Contents lists available at ScienceDirect

Energy Storage Materials

journal homepage: www.elsevier.com/locate/ensm

Moderately concentrated electrolyte improves solid–electrolyte interphase and sodium storage performance of hard carbon

Jagabandhu Patra[a], Hao-Tzu Huang[a], Weijiang Xue[b,c], Chao Wang[b,c], Ahmed S. Helal[b], Ju Li[b,*], Jeng-Kuei Chang[a,b,d,**]

[a] Institute of Materials Science and Engineering, National Central University, Taoyuan, Taiwan, ROC
[b] Department of Nuclear Science and Engineering and Department of Materials Science and Engineering, Massachusetts Institute of Technology, Cambridge, USA
[c] School of Materials Science and Engineering, Tongji University, Shanghai 201804, China
[d] Hierarchical Green-Energy Materials (Hi-GEM) Research Center, National Cheng Kung University, Tainan, Taiwan, ROC

ARTICLE INFO

Keywords:
Sodium-ion battery
Hard carbon
Electrolyte
Solid–electrolyte interphase
Coulombic efficiency
Cyclic stability

ABSTRACT

Hard carbon (HC) is a promising anode for sodium-ion batteries. The current hurdles for the HC electrodes are insufficient coulombic efficiency (CE), rate capability, and cyclic stability. This study reveals that an intelligent electrolyte design can effectively overcome these limitations. The sodium salt, concentration, and solvent of the electrolytes are systematically investigated. Incorporation of ethylene carbonate (EC) in propylene carbonate (PC) electrolyte can promote the formation of contact ion pairs and ion aggregates between Na^+ and FSI^-. At a moderate concentration, the 3 mol dm^{-3} NaFSI in PC:EC electrolyte with reasonable conductivity and viscosity can lead to the formation of a robust organic–inorganic balanced solid–electrolyte interphase, which is thoroughly examined by electrochemical impedance spectroscopy, X-ray photoelectron spectroscopy, and transmission electron microscopy. With this, the first-cycle and steady-state CE of the HC electrode is increased to 85% and > 99.9%, respectively, and the reversible sodiation/desodiation capacities at high rates are markedly improved. In addition, 95% of the initial capacity can be retained after 500 charge–discharge cycles. The proposed electrolyte represents a huge step towards HC electrodes with high effectiveness and durability for electrochemical Na^+ storage.

1. Introduction

Large-scale energy storage has attracted enormous attention, because it is currently a bottleneck with regard to enabling the use of intermittent renewable energy, such as solar and wind power [1]. The Li-ion batteries (LIBs), which are widely used for consumer electronic devices and electric vehicles, may not be a good candidate for this application, due to the uneven distribution of Li in the earth's crust [2]. Li is also an important ingredient for glass, ceramic, and the pharmaceutical industries, which are expected to grow at a rapid pace [3,4]. Even worse, political issues can affect the stability of the Li supply. In this context, one of the most appealing alternatives or complements is to use highly abundant Na [5–7]. Recently, several promising Na-ion battery (NIB) cathodes, including layered oxides, polyanionic compounds, Prussian blue analogues, and organic compounds have been reported [8–13], with the performance being close to that of LIB cathodes [5]. Finding a good anode is more challenging, since the commonly used LIB graphite anode has poor Na^+ storage capability, due to the large diameter of Na^+ (1.02 Å vs. 0.76 Å for Li^+) and the lack of stable graphite intercalation compounds for Na^+ [14,15]. While Ti-based compounds usually have low capacities, alloying and conversion electrodes typically suffer from unsatisfactory reversibility and cyclic stability, and thus carbonaceous anodes seem to be the materials that have so far proved practically viable [16–18]. Hard carbon (HC) is probably the most favorable of these from an application viewpoint, because the low cost and easy accessibility are in line with the NIB philosophy (in which cost-effectiveness and large-scale energy storage are major concerns). More research into HC is urgently required, as further performance improvement for the HC anode will be an enabling step for the practical implementation of NIBs.

Currently HC anodes encounter three obstacles in NIBs. First is the low first-cycle coulombic efficiency (CE), which causes a large penalty in the cell energy density [7,17]. In a full cell, the cyclable Na^+ is provided by the positive electrode. The high coulombic inefficiency

* Correspondence to: Massachusetts Institute of Technology, 77 Massachusetts Ave, Cambridge, MA 02139, USA.
** Correspondence to: National Central University, 300 Jhong-Da Road, Taoyuan, Taiwan, ROC.
E-mail addresses: liju@mit.edu (J. Li), jkchang@ncu.edu.tw, jkchang@mit.edu (J.-K. Chang).

https://doi.org/10.1016/j.ensm.2018.04.022
Received 15 December 2017; Received in revised form 19 April 2018; Accepted 19 April 2018
Available online 25 April 2018
2405-8297/

(CI≡1-CE) means large irreversible consumption of the available Na^+, decreasing the cell performance. Of note, in order to prevent metallic Na deposition during charging, a practical cell is assembled with an excess-capacity anode, which would worsen the situation still. This is one reason for the inferior energy density of NIBs compared to that of LIBs, where the graphite anodes with a first-cycle CE of ~ 90% are common in LIBs. Second: the unsatisfactory charge–discharge kinetics, which limits the cell rate capability. While the cathodes are able to operate at a high rate (e.g., 100 C for $Na_3V_2(PO_4)_3$ and 150 C for $NaCrO_2$) [19,20], the sodiation/desodiation reaction for HC electrodes is relatively sluggish. As a result, the HC side is the bottleneck (or the rate-limiting electrode) for the cell power density. Third: the insufficient cycle life, which restricts the end-of-life total energy that can be stored/released. This has been attributed to the less than ideal surface passivation at the HC electrode, as compared to that formed in LIBs [21,22]. Many research efforts have been devoted to mastering the HC microstructure–property relations [17]. Nevertheless, the electrolyte that is adopted, and thus the solid–electrolyte interphase (SEI) created, is as crucial with regard to HC electrodes overcoming these limitations.

The electrolyte plays a crucial role in determining the battery charge–discharge CE, internal impedance (including the ion transport and SEI resistances), cycle life, thermal stability, and safety properties of such devices [23,24]. For the Na salts, Alcántara et al. showed that $NaClO_4$ is better than $NaPF_6$ in dimethyl carbonate (DMC): ethylene carbonate (EC) electrolyte for a carbon electrode, in terms of reversible capacities [25]. Ponrouch et al. reported a similar trend ($NaClO_4$ > $NaPF_6$) in propylene carbonate (PC):EC electrolyte [23]. However, different results were found according to Komaba et al., who indicated that $NaPF_6$ and $NaN(SO_2CF_3)_2$ enabled a greater HC capacity and better cycle performance than $NaClO_4$ did in PC electrolyte [26,27]. On the other hand, effects of solvents were studied using tetrahydrofuran (THF), THF:EC, DMC:EC, and dimethyl ether containing $NaClO_4$ [28], with the first solvent being optimal. Later, PC, PC:EC, and diethyl carbonate (DEC):EC electrolytes (with $NaClO_4$) were found to be suitable electrolytes to ensure high CE and high stability for HC electrodes [23,26]. Besides, super-concentrated electrolytes have lately received considerable attention for use in LIBs and NIBs [29–32]. With this new approach, expansion of the electrolyte electrochemical stability potential window and suppression of both the Al current collector and active material dissolution have been reported [33]. At high concentration, the salt anions are predominantly reduced to form an anion-derived SEI, in contrast to the solvent-derived SEI found for the conventional dilute electrolyte, at the electrode surface [29,32,34]. The former kind of SEI has been proven to possess enhanced passivation ability [32,35]. But the ultra-high concentration (e.g., up to 10 M) also creates some problems. For instance, the increased cost due to the large quantity of salt is particularly undesirable for NIBs, where cost considerations are key. Moreover, the resulting high viscosity impairs the electrolyte penetration and ion transport, especially for thick electrodes. The wettability of this super-concentrated electrolyte towards separators is also an issue. Developing an intelligent electrolyte formulation with an optimal salt concentration that can maximize the NIB performance is the target of this work.

In the first part of the present study, $NaClO_4$, $NaPF_6$, and $NaN(SO_2F)_2$ (sodium bis(fluorosulfonyl)imide; NaFSI) salts in various carbonate solvents are investigated for the HC electrodes, because alkyl carbonate is the most mature solvent to date, and has the most balanced overall performance for LIBs and NIBs [3,36,37]. Since the NaFSI in PC-based electrolyte is particularly promising, in the second part of this work we systematically study the 1–3 mol dm^{-3} NaFSI in PC and PC:EC electrolytes. The EC effects on the concentration-dependent charge–discharge performance are emphasized. With a moderate NaFSI concentration and EC incorporation, a unique and robust SEI can be formed. The resulting excellent first-cycle CE, rate capability, and cyclic stability of the HC electrode are confirmed.

2. Experimental procedures

2.1. Materials and cell assembly

The HC was obtained from Kureha Co. (Carbotron P) and used as received. The electrolytes were prepared by dissolving different salts ($NaClO_4$, $NaPF_6$, or NaFSI, 99.7%) as per the required concentrations in various solvents (DEC:EC (1:1 by volume), PC, or PC:EC (1:1 by volume)) at 25 °C. All the salts were dried in a vacuum at 100 °C for 24 h, and the solvents were dried over fresh molecular sieves for two days, resulting in the water contents of all electrolytes being below 10 ppm, as measured using a Karl-Fischer titrator. To prepare the HC electrode, a slurry made up of 70 wt% active material, 20 wt% carbon black (Cabot Corporation), and 10 wt% poly(vinylidene fluoride) in *N*-methyl-2-pyrrolidone solution was pasted onto Cu foil. This electrode was vacuum-dried at 100 °C for 3 h, roll-pressed, and then punched to match the required dimensions of a CR2032 coin cell. The HC loading amount was 1–1.2 mg cm^{-2}. Thick Na foil and a glassy fiber membrane were used as the counter electrode and separator, respectively. The assembly of the coin cells was performed in an argon-filled glove box (Innovation Technology Co. Ltd.), where both the moisture and oxygen contents were maintained at below 0.5 ppm. We found that the carbon black also participated in the sodiation/desodiation reaction. Accordingly, the reported specific capacities in this work are based on the total weight of HC and carbon black.

2.2. Material and electrochemical characterizations

The ionic conductivity and viscosity of the electrolytes were measured using a TetraCon 325 conductivity meter and a Brookfield DV–I viscometer, respectively, at 25 °C. The crystallinity and morphology of the HC were characterized by X-ray diffraction (XRD, Bruker D8 ADVANCE) and scanning electron microscopy (SEM, FEI Inspect F50), respectively. A Raman spectrometer (UniRAM Micro Raman; λ = 532 nm) was used to study the coordination states of various electrolytes. Electrochemical impedance spectroscopy (EIS) was conducted in a frequency range of 100 kHz–10 mHz and an AC amplitude of 10 mV. The charge–discharge properties (such as capacity, rate capability, and cyclic stability) of various cells were evaluated using a battery tester (Arbin, BT–2043) at 25 °C. For each condition, at least five cells were measured. The performance deviation was typically within 5%, and the reported data are the median values. Some selected HC electrodes, after being cycled at a rate of 0.03 A g^{-1} for five times, were dissembled from the coin cells and washed with PC solvent in the glove box. These electrodes were then transferred to the X-ray photoelectron spectroscopy (XPS, VG Sigma Probe) analytic chamber using an air-tight vessel, which prevented the samples from being exposed to air. High-resolution transmission electron microscopy (TEM; JEOL 2100F) was also used to observe the HC powder scraped off from the cycled electrodes.

3. Results and discussion

The morphology of the HC used is shown in Fig. 1(a). It has an irregular shape, with the particle size mainly ranging from 5 to 10 μm. The Brunauer–Emmett–Teller (BET) surface area was measured to be ~ 6 m^2 g^{-1}. The XRD pattern in Fig. 1(b) reveals the low crystallinity of the HC, which reflects the lack of a long-range order of carbon atoms. According to the diffraction angle, the average *d*-spacing between the carbon layers is ~ 0.385 nm. These material characteristics are consistent with those of the typical HC for battery applications.

First, various electrolyte formulations were examined with the concentration fixed at 1 mol dm^{-3} solvent. $NaClO_4$ in DEC:EC, probably the most commonly used electrolyte in the NIB literature, was used. $NaPF_6$ in PC:EC, which has been considered a promising electrolyte for HC electrodes was also adopted [23]. Moreover, the

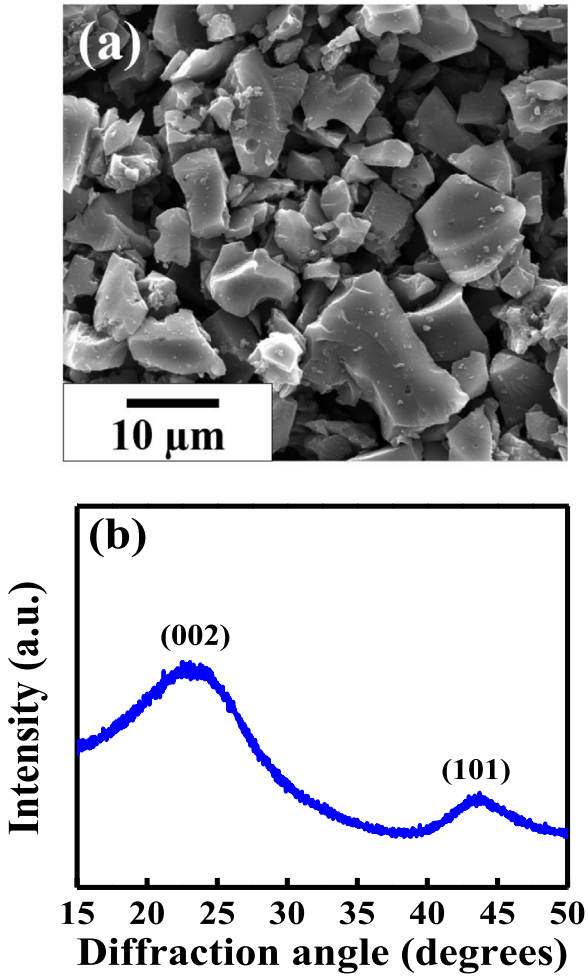

Fig. 1. (a) SEM image and (b) XRD pattern of HC powder.

NaFSI salt, characterized by great chemical and thermal stabilities and low cation-anion binding energy [36,38], was dissolved in DEC:EC, PC, and PC:EC solvents as another three electrolytes. Fig. 2(a) shows the initial five charge–discharge curves of the HC electrode recorded in 1 mol dm^{-3} $NaClO_4$/DEC:EC electrolyte (the data measured in the other electrolytes are shown in Fig. S1). In the first charge (sodiation), an irreversible reduction reaction occurred below 1 V, which was associated with electrolyte decomposition and SEI formation [39], resulting in CE loss. Fig. 2(b) compares the CE values in various electrolytes. The $NaClO_4$/DEC:EC electrolyte showed a distinctly lower CE, being ~ 57% at the first cycle and ~ 96% at the fifth, indicating insufficient passivation of the electrode. Moreover, $NaClO_4$ poses explosion hazards [23,36]; this electrolyte is thus considered inadequate for HC electrodes. It was found that the initial CE values for NaFSI/DEC:EC (61%), NaFSI/PC (62%), and NaFSI/PC:EC (64%) are higher than that (59%) for $NaPF_6$/PC:EC. The NaFSI salt together with PC:EC solvent is for the first time confirmed to be able to create a superior SEI. At the fifth cycle, an ideal CE of ~99.2% was achieved at a low rate of 0.03 A g^{-1}. As shown in Fig. 2(c), after five conditioning cycles all charge–discharge profiles are characterized by a sloping region (1.2–0.1 V) and a plateau region (below 0.1 V), which are consistent with the literature results [16,23,26,27]. The former is attributed to the Na^+ insertion in the carbon layers, whereas the latter is associated with filling of Na^+ into the HC micropores [26]. The reversible desodiation capacities found in the $NaClO_4$/DEC:EC, $NaPF_6$/PC:EC, NaFSI/DEC:EC, NaFSI/PC, and NaFSI/PC:EC electrolytes were 205, 214, 191, 210, and 218 mA h g^{-1}, respectively. The capacities of the HC electrodes measured at various rates in four electrolytes are summarized in Table S1. The electrolyte compositions do play a role in determining the electrode charge–discharge performance.

Based on the results above, we further investigated the concentration effects of NaFSI in both PC and PC:EC electrolytes. Fig. 3 shows the conductivity and viscosity of the electrolytes. The plain PC and PC:EC solvents showed the viscosity values of 2.4 and 2.0 cP, respectively. It was found that the EC incorporation improved the ionic conductivity and decreased electrolyte viscosity, regardless of the salt concentration. In PC:EC solvent, the conductivity decreased from 8.8 mS cm^{-1} (for 1 mol dm^{-3}) to 6.3 mS cm^{-1} (for 3 mol dm^{-3}), and the viscosity increased from 4 cP (for 1 mol dm^{-3}) to 22 cP (for 3 mol dm^{-3}), with NaFSI salt. It is noted that at the moderate concentration of 3 mol dm^{-3}, the conductivity and viscosity are still satisfactory for battery applications. The electrolyte can easily penetrate the separator and HC electrode (see Fig. S2). When the concentration increased to 4 mol dm^{-3}, the NaFSI salt can initially be dissolved. However, precipitation was observed after 12 h (see Fig. S3), probably due to a temperature variation. This indicates that the solubility of NaFSI in this solvent is near 4 mol dm^{-3}.

Raman spectroscopic analyses were conducted to gain insight into the coordination structures of the electrolytes. As shown in Fig. 4, various vibrational modes of FSI^- are found in the range of 680–780 cm^{-1}, depending on the coordination states. The band at ~ 724 cm^{-1} is assigned to free FSI^- anions (i.e., in a solvent-separated state) without direct interaction with cations [40]. When a FSI^- is coordinated with one or more Na^+ cations, forming a contact ion pair (CIP) or an aggregate (AGG), the band shifts to ~ 734 or ~ 742 cm^{-1} [41,42]. The blank PC and PC:EC solvents show signals at ~ 716 and ~ 722 cm^{-1}, respectively. With increasing NaFSI concentration, the solvent and free FSI^- signals decreased, whereas the CIP and AGG ratios gradually increased. Of note, although the exact cause is not yet clear, EC incorporation did shift the spectra towards a higher wavenumber. As shown in the figure, at 3 mol dm^{-3}, EC clearly promoted the formation of CIPs and AGGs. Further experimental and simulation works are needed to clarify the mechanism.

Fig. 5(a) reveals the effects of NaFSI concentration and EC addition on the initial charge–discharge behavior of the HC electrodes. At the concentration of 1 mol dm^{-3}, the electrolyte with EC rendered a higher potential plateau upon charging, which was related to the preferential decomposition of EC at the electrode [43]. With increasing the concentration, regardless of the solvent types, the charging curves clearly shifted towards lower potential due to the reduced amount (and thus activity) of solvent. It was proposed that in the CIP and AGG states (rather than the free FSI^- state), the FSI^- anions can partially donate their electrons to Na^+ cations and thus have less negative charges. As a result, the FSI^- anions become more susceptible to reduction [32,33,44]. The more detailed mechanism has been discussed on the basis of frontier orbital calculation, which indicates that the LUMO is located on the FSI^- anions due to the downward shift of the FSI^- orbital level in the CIP and AGG states [29,44]. This leads to formation of an anion-derived SEI film with great passivation ability. This argument is supported by Fig. S4, which reveals a clear oxidation of Na foil in the 1 mol dm^{-3} electrolytes, whereas the same foil remained fresh after immersion in the 3 mol dm^{-3} electrolytes for 5 days. As shown in Fig. 5(b), the first-cycle CE values recorded in 1 mol dm^{-3} NaFSI/PC, 1 mol dm^{-3} NaFSI/PC:EC, 3 mol dm^{-3} NaFSI/PC, and 3 mol dm^{-3} NaFSI/PC:EC at a rate of 0.03 A g^{-1} were 62%, 64%, 75%, and 85%; they increased to 99.2%, 99.2%, 99.5%, and 99.8%, respectively, at the fifth cycles. Interestingly, the EC incorporation and high NaFSI concentration seem to have a synergistic effect in improving the SEI effectiveness, and the details of this will be discussed later. The huge first-cycle CE increase as compared to that (~ 59%) for commonly adopted electrolyte (1 mol dm^{-3} $NaPF_6$/PC:EC) will lead to a significant improvement in the full cell energy density.

The charge–discharge curves measured in the PC and PC:EC electrolytes with various NaFSI concentrations are shown in Fig. S5.

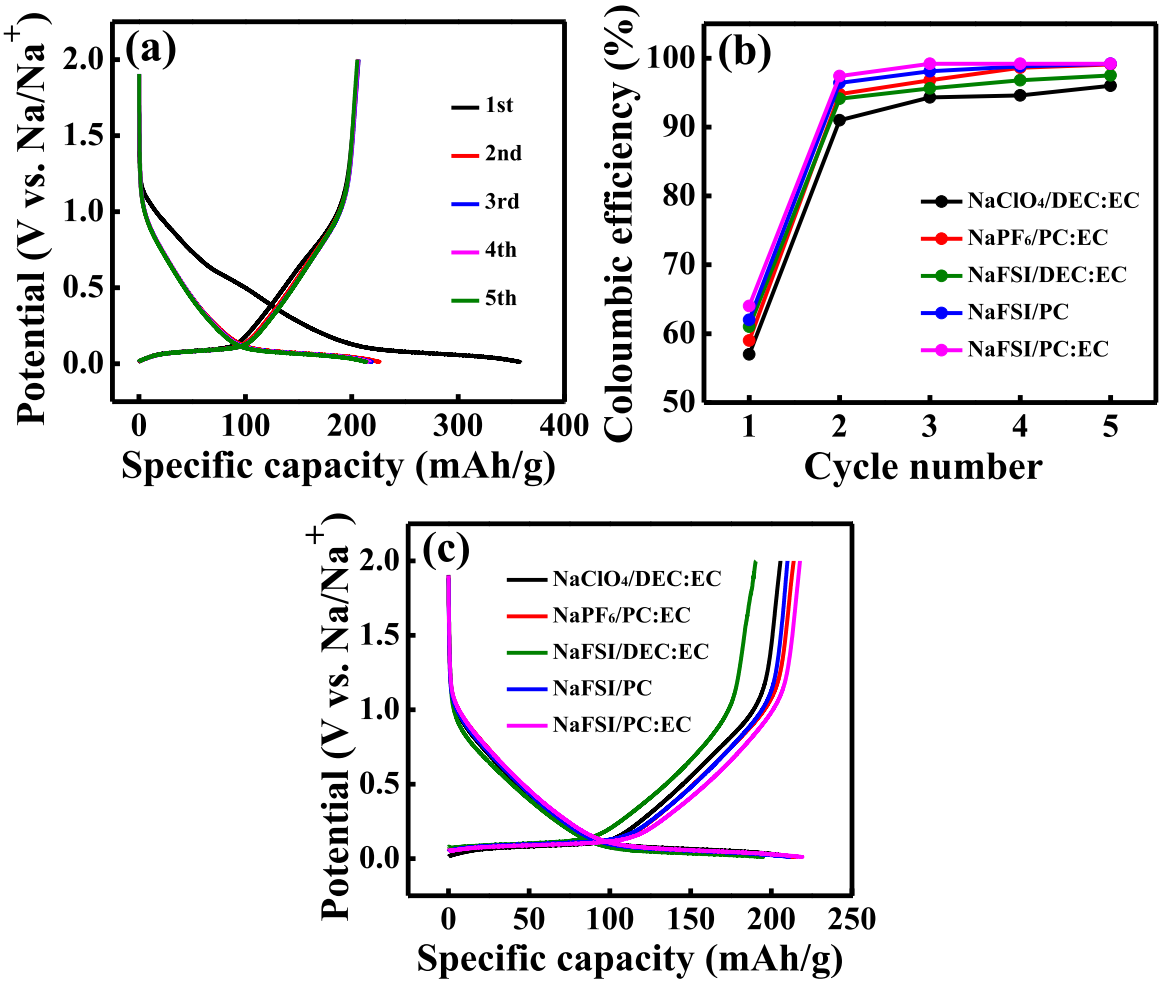

Fig. 2. (a) Initial five charge–discharge curves of HC electrode recorded in 1 mol dm^{-3} $NaClO_4$/DEC:EC electrolyte. (b) The CE values of initial five cycles recorded in various 1 mol dm^{-3} electrolytes. (c) Charge–discharge curves (after conditioning cycles) of HC electrodes recorded in various electrolytes. All the data were measured at 0.03 A g^{-1}.

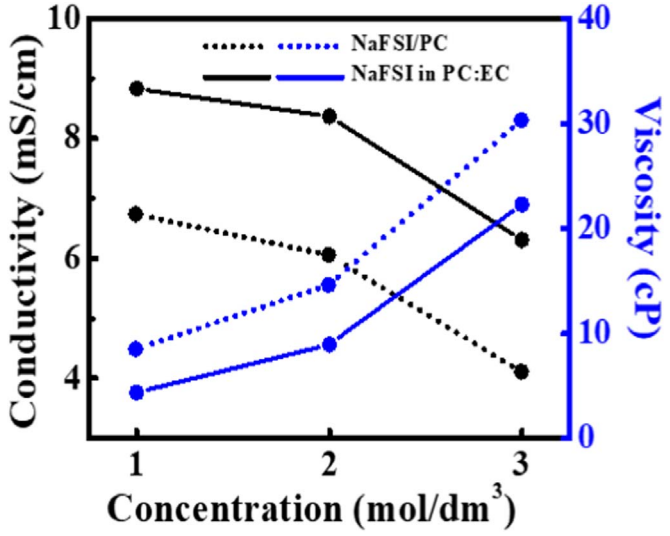

Fig. 3. Conductivity and viscosity of PC and PC:EC electrolytes with various concentrations of NaFSI.

The capacities obtained at various rates are compared in Fig. 6(a) and Table S2. All the capacities measured in the 2 mol dm^{-3} electrolytes were between those of the 1 and 3 mol dm^{-3} electrolytes, so they are not presented in Fig. 6(a). The reversible capacities measured at 0.03 A g^{-1} in 1 mol dm^{-3} NaFSI/PC, 1 mol dm^{-3} NaFSI/PC:EC, 3 mol dm^{-3} NaFSI/PC, and 3 mol dm^{-3} NaFSI/PC:EC electrolytes were 210, 218, 237, and 253 mA h g^{-1}, respectively. At 1 A g^{-1}, 31%, 34%, 36%, and 45% of these capacities can be retained. Fig. 6(b) shows the EIS data of the HC electrodes in various electrolytes. The Nyquist spectra are composed of a semicircle at high frequency and a sloping line at low frequency, which can be characterized by the equivalent circuit shown in the figure inset, where R_e, R_{ct}, CPE and W are the electrolyte resistance, interfacial charge transfer resistance, interfacial constant phase element, and Warburg impedance associated with Na^+ diffusion in the electrode, respectively [45]. The apparent Na^+ diffusion coefficients (D_{Na^+}) for the electrodes can be calculated from the oblique linear Warburg parts according to the literature [46]. As shown in Table 1, the electrolytes with a higher NaSFI concentration and EC addition have lower R_{ct} and larger D_{Na^+} values. This suggests that the Na^+ in 3 mol dm^{-3} NaFSI/PC:EC electrolyte is relatively easy to be dissociated (from the coordinated solvents and anions) and transported through the SEI, explaining the superior charge–discharge performance found in Fig. 6(a).

It was found that the carbon black also contributed to the electrode capacity. For example, the measured capacities in 3 mol dm^{-3} NaFSI/PC:EC electrolyte were 100 and 45 mA h g^{-1}, respectively, at 0.03 and 1 A g^{-1} (see Fig. S6). Although the HC played the major role in the sodiation/desodiation reaction, the contribution of carbon black to the capacities should not be ignored.

XPS analyses were conducted to further explore the SEI chemistry at the electrode surface. It was already reported that the high salt concentration led to formation of an SEI enriched by the anion

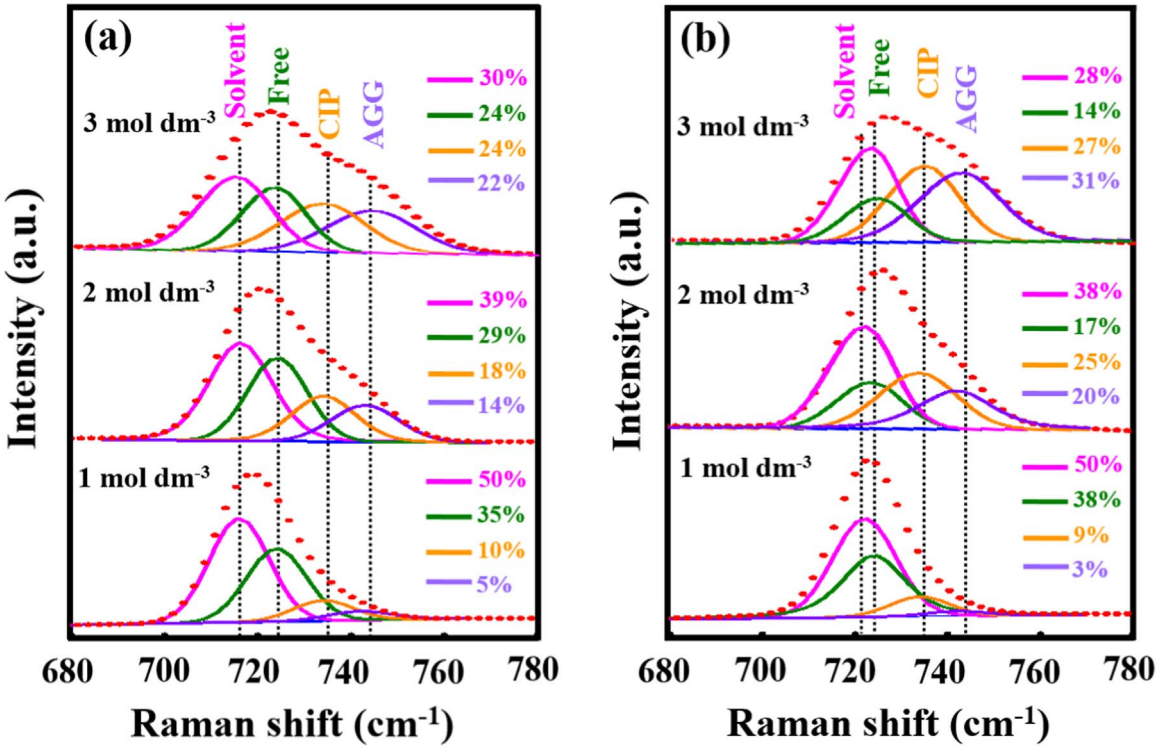

Fig. 4. Raman spectra of (a) PC and (b) PC:EC electrolytes with various concentrations of NaFSI.

decomposition products [29,32]. Therefore, we focus on the EC effects here. Fig. 7(a)–(c) show the XPS C 1s, F 1s, and S 2p spectra obtained for the HC electrodes cycled in 3 mol dm^{-3} NaFSI/PC and 3 mol dm^{-3} M NaFSI/PC:EC electrolytes. Both the F 1s spectra showed a strong signal (at ~ 684.5 eV) related to NaF, which is believed to be a major component of the SEI films. The high binding energy peak (~ 687 eV) is attributed to an F–C bond (from binder) or an F–S bond (from residual FSI). For the C spectrum taken in 3 mol dm^{-3} NaFSI/PC electrolyte, it is relatively enriched with C–O, O–C=O, and CO_3. In contrast, the polyolefin ($(CH_2)_n$) is the main species for the 3 mol dm^{-3} NaFSI/PC:EC spectrum [47]. It is noted that the O–C=O and CO_3 compounds were considered unfavorable for the ion transport and desolvation reaction of Na^+ [48,49], likely contributing to the relatively low performance of the 3 mol dm^{-3} NaFSI/PC cell. As for the sulfur spectra, there are three constituents coexisting: -SO_2- (168.0 and 169.2 eV), -SO_x- (165.9 and 167.1 eV), and sulfide (161.5 and 162.6 eV) [32]. The first species is related to the residual salt [32], whereas the latter two are associated with the reductive decomposition products of FSI^- anions [50,51]. It has been proposed by simulation study that the decomposition of FSI^- begins with the cleavage of the S–F bond, producing $F\cdot^-$ and $F(SO_2)_2N\cdot$ radicals [51,52]. The latter would subsequently undergo N–S bond cleavage and eventually yields -SO_x- and sulfide. The spectrum for NaFSI/PC:EC exhibits much higher concentrations of -SO_x- and sulfide, indicating that the anion decomposition is promoted by the EC addition, given that the amounts of residual salt should be similar for both samples. This is in line with the Raman results which indicated that EC incorporation enhanced the formation of CIPs and AGGs, which should favor anion decomposition upon reduction [33]. Fig. 7(d) compares the surface chemical compositions of the two electrodes. Interestingly, the PC:EC electrolyte derived SEI showed a considerably higher C concentration, presumably due to the easier reduction of EC [43]. In contrast to the inorganic NaF-dominant SEI formed in the PC electrolyte, this unique organic–inorganic balanced film is thus a key for obtaining superior electrochemical performance.

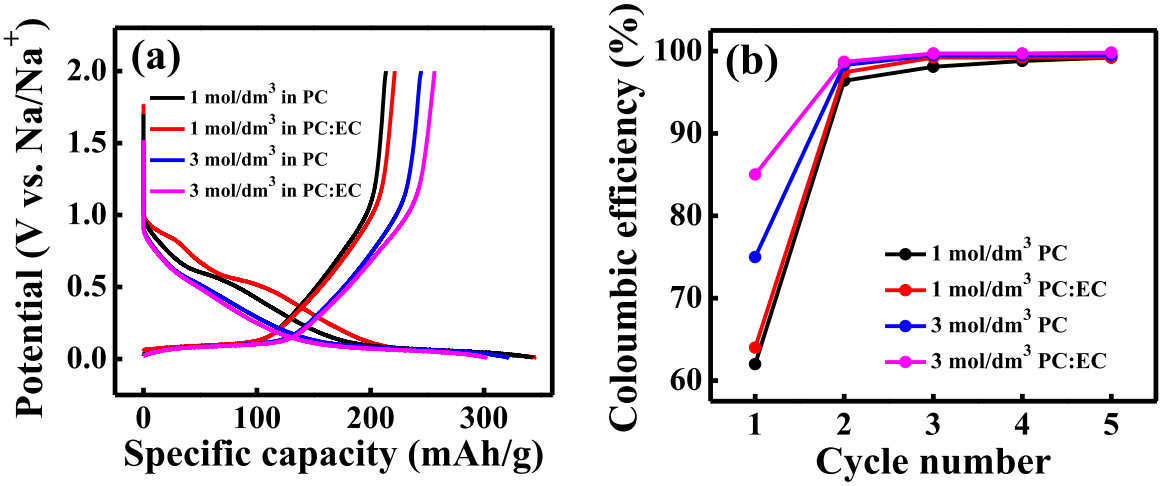

Fig. 5. (a) Initial charge–discharge curves and (b) the CE values of initial five cycles of HC electrodes recorded in various NaFSI electrolytes at 0.03 A g^{-1}.

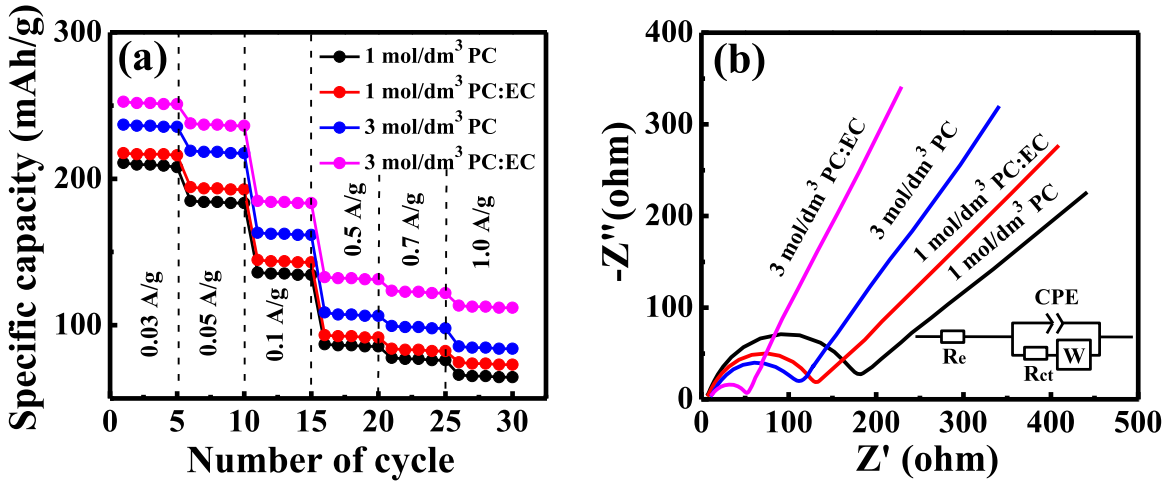

Fig. 6. (a) Capacities of HC electrodes measured in various NaFSI electrolytes at various rates. (b) EIS data of the HC electrodes measured in various NaFSI electrolytes after conditioning cycles.

Table 1
R_{ct} and D_{Na^+} values for HC electrodes measured in various electrolytes after 5 conditioning cycles and 500 charge–discharge cycles.

	After conditioning cycles		After 500 cycles	
	R_{ct} (Ω)	D_{Na^+} ($cm^2\ s^{-1}$)	R_{ct} (Ω)	D_{Na^+} ($cm^2\ s^{-1}$)
1 mol dm^{-3} NaFSI/PC	182	1.1×10^{-11}	515	1.2×10^{-12}
2 mol dm^{-3} NaFSI/PC	147	2.0×10^{-10}	435	8.1×10^{-11}
3 mol dm^{-3} NaFSI/ PC	125	3.5×10^{-10}	365	1.8×10^{-10}
1 mol dm^{-3} NaFSI/ PC:EC	140	1.6×10^{-11}	200	7.2×10^{-12}
2 mol dm^{-3} NaFSI/ PC:EC	80	4.1×10^{-10}	100	2.7×10^{-10}
3 mol dm^{-3} NaFSI/ PC:EC	50	6.3×10^{-10}	60	5.1×10^{-10}

The cycling stability of the electrodes was evaluated with a charge–discharge rate of 0.1 A g^{-1} for 500 cycles. The data in Fig. 8(a) shows that the HC electrodes retained 75%, 78%, 84%, and 95% of their initial capacities in 1 mol dm^{-3} NaFSI/PC, 1 mol dm^{-3} NaFSI/PC:EC, 3 mol dm^{-3} NaFSI/PC, and 3 mol dm^{-3} NaFSI/PC:EC, respectively. Fig. 8(b) shows the EIS data acquired after cycling. As compared to those in Fig. 6(b), the diameters of the semicircles increase (i.e., increase in R_{ct}) and the slopes of the Warburg lines decrease (i.e., decrease in D_{Na^+}) upon cycling. This can be attributed to the accumulation of surface obstacle SEI layers, leading to the capacity decay. Table 1 reveals that the degrees of the R_{ct} and D_{Na^+} degradation depend on the electrolyte composition. Clearly, the stability improved with increasing the salt concentration and the incorporation of EC. With only slight changes in R_{ct} and D_{Na^+}, the HC electrode showed excellent cyclability in 3 mol dm^{-3} NaFSI/PC:EC electrolyte, with a 0.01% capacity decay on average per charge–discharge cycle. The unique organic–inorganic composite SEI layer formed in this electrolyte is highly robust and enables a high CE of > 99.9% during cycling. Owing to the great passivation, irreversible side reactions were minimized, resulting in extraordinary electrode durability. This conclusion is supported by the TEM bright-field image shown in Fig. 9. While the SEI formed in 3 mol dm^{-3} NaFSI/PC electrolyte after cycling is discontinuous and much thicker (up to ~ 20 nm), the SEI formed in 3 mol dm^{-3} NaFSI/PC:EC electrolyte is compact and well adhered, with a thickness of ~ 5 nm. Presumably, the former inorganic-rich SEI is relatively brittle, and thus is easily fractured upon electrode volume variation during sodiation/desodiation. The repeated breakdown and growth of the SEI made it become thicker and nonuniform, increasing the electrode impedance upon cycling. This is considered a crucial factor in determining the electrode charge–discharge performance. It is noted that in this study we did not use electrode post-treatment, functional binder, or electrolyte additives, which are known to be beneficial for electrode cyclic stability [53–56]. This indicates that our electrolyte design approach is highly effective, and also implies that the performance could be further improved by combining with the other strategies. Fig. S7 compares the flammability of the proposed 3 mol dm^{-3} NaFSI/PC:EC electrolyte and the conventional 1 mol dm^{-3} $NaPF_6$/PC:EC electrolyte. Glass fiber papers were used to absorb the electrolytes and then tested with an electric Bunsen burner under air. The former electrolyte burned much less violently due to the reduced concentration of solvent molecules, which are mainly coordinated with Na^+ (i.e., the amount of free solvent is limited). The lower volatility and reactivity are highly desirable for improving the intrinsic safety properties of the electrolyte.

It is noted that our electrolyte concentration is considerably lower than that of super-concentrated electrolytes used in the literature (e.g., up to 10 M) [29,31,57,58]. A very recent paper [59] used 3.3 M NaFSI/trimethyl phosphate electrolyte, which is still more concentrated than our electrolyte (3 mol dm^{-3} = ~ 2.45 M for NaFSI/PC:EC). Our key finding is that the EC incorporation can promote formation of CIPs and AGGs in the electrolyte; therefore, the super-high salt concentration is not required. This concept (moderate concentration with EC) is for the first time proposed and is helpful to reduce the cost of the electrolyte (vs. super-concentrated electrolytes). The normal-concentration EC based electrolytes with a fluoroethylene carbonate (FEC) additive was found to enable high electrode cyclability [60–62]; however, the FEC reduced the capacity and first-cycle CE and increased the electrode polarization during charging/discharging [62,63]. Using the proposed moderately-concentrated electrolyte can be a cost-effective method to optimize the overall performance of HC electrodes. We further tested the compatibility of this electrolyte (3 mol dm^{-3} NaFSI/PC:EC) with a thick HC electrode (with a loading amount of 11.5 mg cm^{-2}). As shown in the supplementary video, the electrolyte can easily and quickly wet the electrode. Moreover, satisfactory charge–discharge performance is shown in Fig. S8. Although the high-rate capability is inferior to that of the thin electrode (e.g., 83 vs. 114 mA h g^{-1} at a rate of 1 A g^{-1}), the results indicate that the proposed electrolyte is really useful for the electrode with practical thickness.

Supplementary material related to this article can be found online at http://dx.doi.org/10.1016/j.ensm.2018.04.022.

4. Conclusions

Through systematic investigations, the synergistic effects of NaFSI concentration and EC addition in the PC electrolyte on the SEI

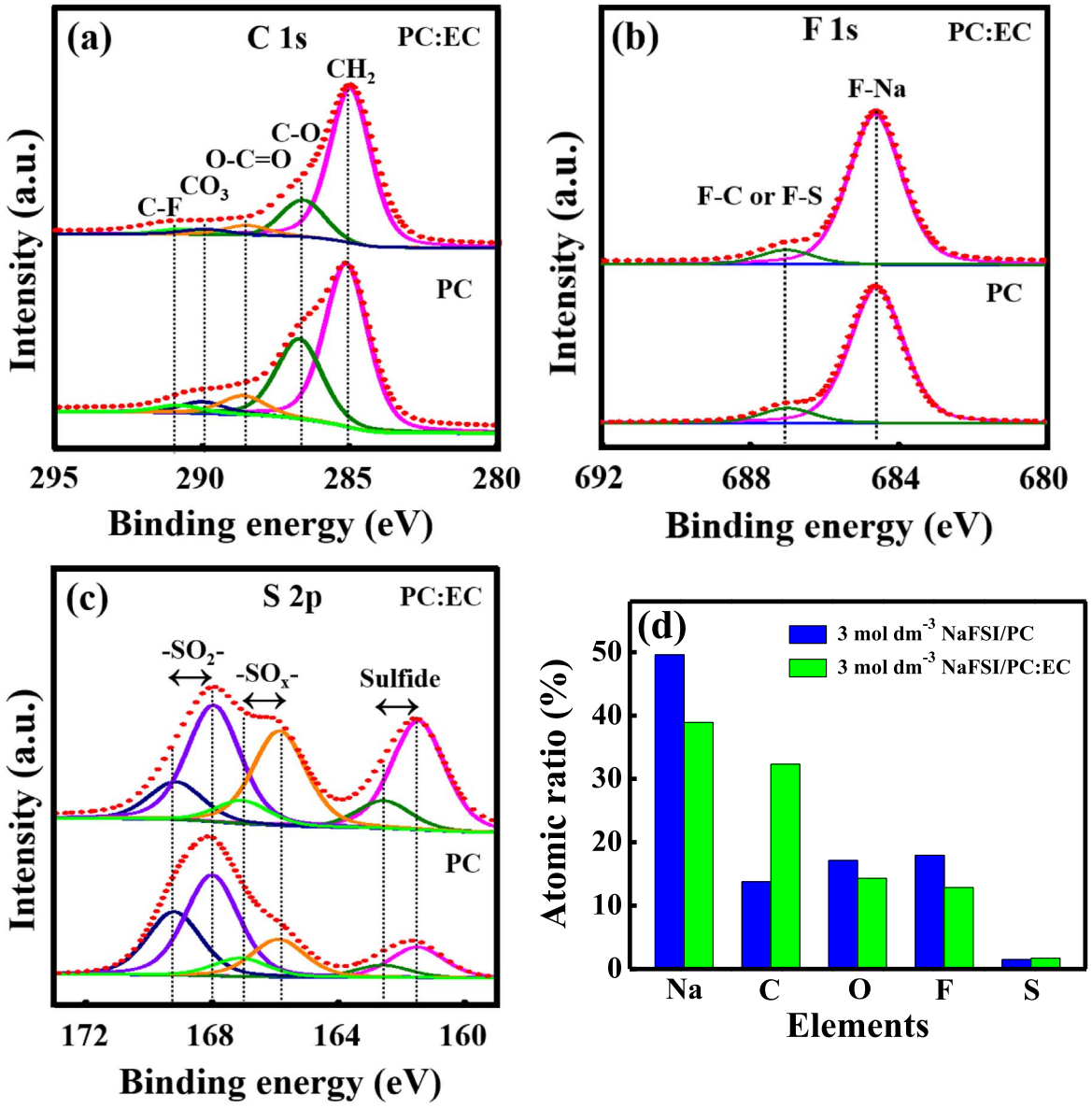

Fig. 7. XPS (a) C 1s, (b) F 1s, and (c) S 2p spectra for HC electrodes cycled in 3 mol dm^{-3} NaFSI/PC and 3 mol dm^{-3} M NaFSI/PC:EC electrolytes. (d) Surface chemical composition comparisons of the two electrodes.

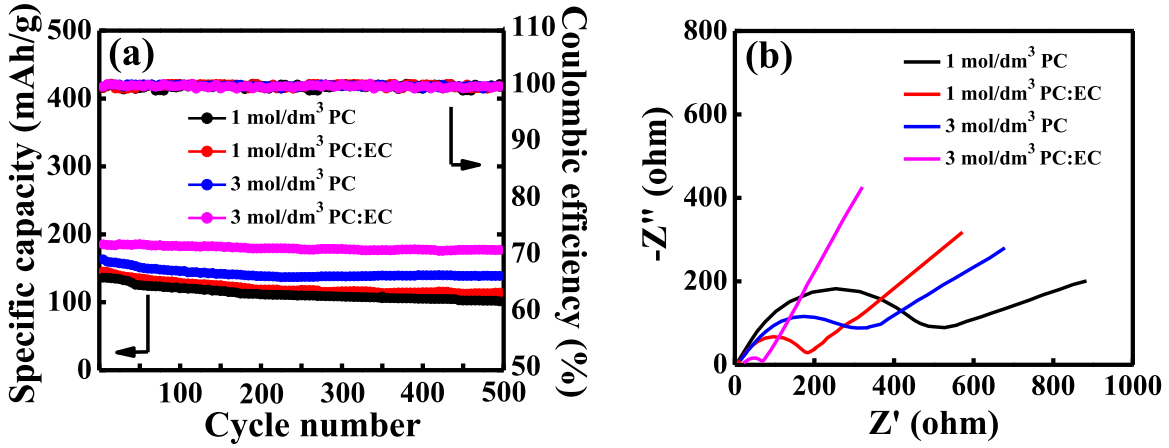

Fig. 8. (a) Cyclic stability data of HC electrodes measured in various NaFSI electrolytes at 0.1 A g^{-1}. (b) EIS data of the HC electrodes measured in various NaFSI electrolytes after 500 cycles.

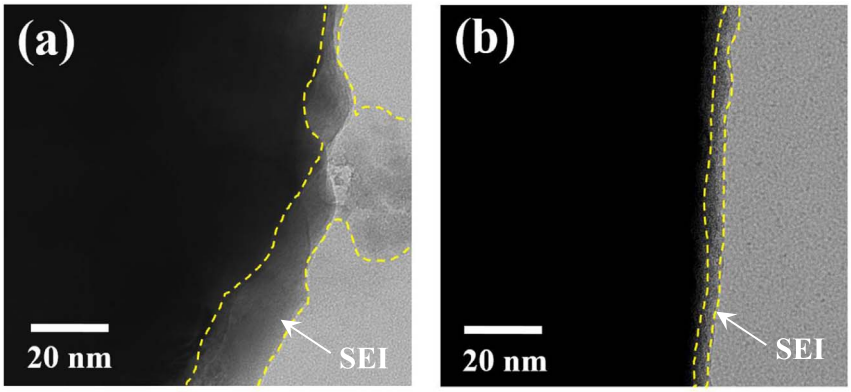

Fig. 9. TEM bright-field images of HC powder after being cycled in (a) 3 mol dm^{-3} NaFSI/PC and (b) 3 mol dm^{-3} M NaFSI/PC:EC electrolytes for 500 times.

chemistry and the corresponding charge–discharge performance of the HC electrodes are explored. The moderately-concentrated 3 mol dm^{-3} NaFSI/PC:EC electrolyte with a satisfactory conductivity of 6.3 mS cm^{-1} and viscosity of 23 cP can well penetrate the separator and HC electrode and show reduced flammability. The EC incorporation promoted the CIP and AGG components in the electrolyte, and led to formation of a robust organic–inorganic balanced SEI (mainly composed of $(CH_2)_n$ and NaF). This SEI not only enables easy charge transfer and fast Na^+ transport, but also shows great passivation ability and excellent durability. With this, the first-cycle CE of the HC electrode can be dramatically increased by > 25%, to 85%. Moreover, with a steady-state CE of > 99.9%, less than 5% capacity decay was measured after 500 charge–charge cycles, when TEM confirmed that the HC surface was covered by a thin (~ 5 nm) and well-adhering SEI layer. The proposed electrolyte design approach is facile and can effectively upgrade the NIB energy density (because the increase in both first-cycle CE and discharge capacity for the HC electrode), power density (because the kinetics of the rate-limited anode is improved), and cycle life.

Acknowledgements

The financial support provided for this work by the Ministry of Science and Technology (MOST) (Grant No. 106-2628-E-008-002-MY3 and 106-2221-E-008-091-MY3) of Taiwan is gratefully appreciated. We also acknowledge support by the Natural Natural Science Foundation of China (Grant No. 51632001). JL acknowledges support by NSF ECCS-1610806.

Data availability statement

The raw/processed data required to reproduce these findings cannot be shared at this time as the data also forms part of an ongoing study.

Appendix A. Supplementary material

Supplementary data associated with this article can be found in the online version at doi:10.1016/j.ensm.2018.04.022.

References

[1] J.Y. Hwang, S.T. Myung, Y.K. Sun, Sodium-ion batteries: present and future, Chem. Soc. Rev. 46 (2017) 3529–3614.
[2] J.W. Choi, D. Aurbach, Promise and reality of post-lithium-ion batteries with high energy densities, Nat. Rev. Mater. 1 (2016) 16013.
[3] A. Ponrouch, D. Monti, A. Boschin, B. Steen, P. Johansson, M.R. Palacın, Non-aqueous electrolytes for sodium-ion batteries, J. Mater. Chem. A 3 (2015) 22–42.
[4] J.M. Tarascon, Is lithium the new gold?, Nat. Chem. 2 (2010) 510.
[5] H. Kim, H. Kim, Z. Ding, M.H. Lee, K. Lim, G. Yoon, K. Kang, Recent progress in electrode materials for sodium-ion batteries, Adv. Energy Mater. 6 (2016) 1600943.
[6] P.K. Nayak, L. Yang, W. Brehm, P. Adelhelm, From Lithium-ion to sodium-ion batteries: advantages, challenges, and surprises, Angew. Chem. Int. Ed. 57 (2017) 102–120.
[7] N. Yabuuchi, K. Kubota, M. Dahbi, S. Komaba, Research development on sodium-ion batteries, Chem. Rev. 114 (2014) 11636–11682.
[8] N. Wongittharom, C.H. Wang, Y.C. Wang, C.H. Yang, J.K. Chang, Ionic liquid electrolytes with various sodium solutes for rechargeable Na/$NaFePO_4$ batteries operated at elevated temperatures, ACS Appl. Mater. Interfaces 6 (2014) 17564–17570.
[9] C.H. Wang, Y.W. Yeh, N. Wongittharom, Y.C. Wang, C.J. Tseng, S.W. Lee, W.S. Chang, J.K. Chang, Rechargeable Na/$Na_{0.44}MnO_2$ cells with ionic liquid electrolytes containing various sodium solutes, J. Power Sources *274* (2015) 1016–1023.
[10] H.Y. Li, C.H. Yang, C.M. Tseng, S.W. Lee, C.C. Yang, T.Y. Wu, J.K. Chang, Electrochemically grown nanocrystalline V_2O_5 as high-performance cathode for sodium-ion batteries, J. Power Sources 285 (2015) 418–424.
[11] W.J. Li, C. Han, W. Wang, F. Gebert, S.L. Chou, H.K. Liu, X. Zhang, S.X. Dou, Commercial prospects of existing cathode materials for sodium ion storage, Adv. Energy Mater. (2017) 1700274.
[12] Y. You, A. Manthiram, Progress in high-voltage cathode materials for rechargeable sodium-ion batteries, Adv. Energy Mater. (2017) 1701785.
[13] H. Zhao, J. Wang, Y. Zheng, J. Li, X. Han, G. He, Y. Du, Organic thiocarboxylate electrodes for a room-temperature sodium-ion battery delivering an ultrahigh capacity, Angew. Chem. Int. Ed. 56 (2017) 15334–15338.
[14] P. Ge, M. Fouletier, Electrochemical intercalation of sodium in graphite, Solid State Ion. 28–30 (1988) 1172–1175.
[15] B. Jache, P. Adelhelm, Use of graphite as a highly reversible electrode with superior cycle life for sodium-ion batteries by making use of co-intercalation phenomena, Angew. Chem. Int. Ed. 53 (2014) 10169–10173.
[16] E. Irisarri, A. Ponrouch, M.R. Palacin, Hard carbon negative electrode materials for sodium-ion batteries, J. Electrochem. Soc. 162 (2015) A2476–A2482.
[17] H. Hou, X. Qiu, W. Wei, Y. Zhang, X. Ji, Carbon anode materials for advanced sodium-ion batteries, Adv. Energy Mater. (2017) 1602898.
[18] K. Kubota, S. Komaba, Review-practical issues and future perspective for Na-ion batteries, J. Electrochem. Soc. 162 (2015) A2538–A2550.
[19] X. Rui, W. Sun, C. Wu, Y. Yu, Q. Yan, An advanced sodium-ion battery composed of carbon coated $Na_3V_2(PO_4)_3$ in a porous graphene network, Adv. Mater. 27 (2015) 6670–6676.
[20] C.Y. Yu, J.S. Park, H. Gi Jung, K.Y. Chung, D. Aurbach, Y.K. Sun, S.T. Myung, $NaCrO_2$ cathode for high-rate sodium-ion batteries, Energy Environ. Sci. 8 (2015) 2019–2026.
[21] D.I. Iermakova, R. Dugas, M.R. Palacin, A. Ponrouch, On the comparative stability of Li and Na metal anode interfaces in conventional alkyl carbonate electrolytes, J. Electrochem. Soc. 162 (2015) A7060–A7066.
[22] R. Mogensen, D. Brandell, R. Youmesi, Solubility of the solid electrolyte interphase (SEI) in sodium-ion batteries, ACS Energy Lett. 1 (2016) 1173–1178.
[23] A. Ponrouch, E. Marchante, M. Courty, J.M. Tarascon, M.R. Palacın, In search of an optimized electrolyte for Na-ion batteries, Energy Environ. Sci. 5 (2012) 8572–8583.
[24] H. Che, S. Chen, Y. Xie, H. Wang, K. Amine, X.Z. Liao, Z.F. Ma, Electrolyte design strategies and research progress for room-temperature sodium-ion batteries, Energy Environ. Sci. 10 (2017) 1075–1101.
[25] R. Alcantara, J.M.J. Mateos, J.L. Tirado, Negative electrodes for lithium-and sodium-ion batteries obtained by heat-treatment of petroleum cokes below 1000 °C, J. Electrochem. Soc. 149 (2002) A201–A205.
[26] S. Komaba, W. Murata, T. Ishikawa, N. Yabuuchi, T. Ozeki, T. Nakayama, A. Ogata, K. Gotoh, K. Fujiwara, Electrochemical Na insertion and solid electrolyte interphase for hard-carbon electrodes and application to Na-ion batteries, Adv. Funct. Mater. 21 (2011) 3859–3867.
[27] M. Dahbi, N. Yabuuchi, K. Kubota, K. Tokiwa, S. Komaba, Negative electrodes for Na-ion batteries, Phys. Chem. Chem. Phys. 16 (2014) 15007–15028.
[28] R. Alcantara, P. Lavela, G.F. Ortiz, J.L. Tirado, Carbon microspheres obtained from resorcinol-formaldehyde as high-capacity electrodes for sodium-ion batteries, Electrochem. Solid-State Lett. 8 (2005) A222–A225.

[29] Y. Yamada, K. Furukawa, K. Sodeyama, K. Kikuchi, M. Yaegashi, Y. Tateyama, A. Yamada, Unusual stability of acetonitrile-based superconcentrated electrolytes for fast-charging lithium-ion batteries, J. Am. Chem. Soc. 136 (2014) 5039–5046.
[30] J. Zheng, J.A. Lochala, A. Kwok, Z.D. Deng, J. Xiao, Research progress towards understanding the unique interfaces between concentrated electrolytes and electrodes for energy storage applications, Adv. Sci. 4 (2017) 1700032.
[31] J. Lee, Y. Lee, J. Lee, S.M. Lee, J.H. Choi, H. Kim, M.S. Kwon, K. Kang, K.T. Lee, N.S. Choi, Ultraconcentrated sodium bis(fluorosulfonyl)imide-based electrolytes for high-performance sodium metal batteries, ACS Appl. Mater. Interfaces 9 (2017) 3723–3732.
[32] K. Takada, Y. Yamada, E. Watanabe, J. Wang, K. Sodeyama, Y. Tateyama, K. Hirata, T. Kawase, A. Yamada, Unusual passivation ability of superconcentrated electrolytes toward hard carbon negative electrodes in sodium-ion batteries, ACS Appl. Mater. Interfaces 9 (2017) 33802–33809.
[33] Y. Yamada, A. Yamada, Superconcentrated electrolytes to create new interfacial chemistry in non-aqueous and aqueous rechargeable batteries, Chem. Lett. 46 (2017) 1056–1064.
[34] Y. Yamada, K. Usui, C.H. Chiang, K. Kikuchi, K. Furukawa, A. Yamada, General observation of lithium intercalation into graphite in ethylene-carbonate-free superconcentrated electrolytes, ACS Appl. Mater. Interfaces 6 (2014) 10892–10899.
[35] M. Nie, D.P. Abraham, D.M. Seo, Y. Chen, A. Bose, B.L. Lucht, Lithium Ion battery graphite solid electrolyte interphase revealed by microscopy and spectroscopy, J. Phys. Chem. C 117 (2013) 1257–1267.
[36] G.G. Eshetu, S. Grugeon, H. Kim, S. Jeong, L. Wu, G. Gachot, S. Laruelle, M. Armand, S. Passerini, Comprehensive insights into the reactivity of electrolytes based on sodium ions, ChemSusChem 9 (2016) 462–471.
[37] V. Etacheri, R. Marom, R. Elazari, G. Salitra, D. Aurbach, Challenges in the development of advanced Li-ion batteries: a review, Energy Environ. Sci. 4 (2011) 3243–3262.
[38] J. Kalhoff, G.G. Eshetu, D. Bresser, S. Passerini, Safer electrolytes for lithium-ion batteries: state of the art and perspectives, ChemSusChem 8 (2015) 2154–2175.
[39] D.A. Stevens, J.R. Dahn, The mechanisms of lithium and sodium insertion in carbon materials, J. Electrochem. Soc. 148 (2001) A803–A811.
[40] A. Boschina, P. Johanssona, Plasticization of NaX-PEO solid polymer electrolytes by $Pyr_{13}X$ ionic liquids, Electrochim. Acta 211 (2016) 1006–1015.
[41] H. Yoon, A.S. Best, M. Forsyth, D.R. MacFarlane, P.C. Howlett, Physical properties of high Li-ion content N-Propyl-N-methylpyrrolidinium bis(fluorosulfonyl)imide based ionic liquid electrolytes, Phys. Chem. Chem. Phys. 17 (2015) 4656–4663.
[42] S.D. Han, O. Borodin, D.M. Seo, Z.B. Zhou, W.A. Henderson, Electrolyte solvation and ionic association V. Acetonitrile-lithium bis (fluorosulfonyl) imide (LiFSI) mixtures, J. Electrochem. Soc. 161 (2014) A2042–A2053.
[43] K. Xu, Nonaqueous liquid electrolytes for lithium-based rechargeable batteries, Chem. Rev. 104 (2004) 4303–4418.
[44] K. Sodeyama, Y. Yamada, K. Aikawa, A. Yamada, Y. Tateyama, Sacrificial anion reduction mechanism for electrochemical stability improvement in highly concentrated Li-salt electrolyte, J. Phys. Chem. C 118 (2014) 14091–14097.
[45] J. Patra, H.C. Chen, C.H. Yang, C.T. Hsieh, C.Y. Su, J.K. Chang, High dispersion of 1-nm SnO_2 particles between graphene nanosheets constructed using supercritical CO_2 fluid for sodium-ion battery anodes, Nano Energy 28 (2016) 124–134.
[46] L. Fan, X. Li, B. Yan, J. Feng, D. Xiong, D. Li, L. Gu, Y. Wen, S. Lawes, X. Sun, Controlled SnO_2 crystallinity effectively dominating sodium storage performance, Adv. Energy Mater. 6 (2016) 1502057.
[47] A. Ponrouch, R. Dedryvere, D. Monti, A.E. Demet, J.M.A. Mba, Le Croguennec, C. Masquelier, P. Johansson, M.R. Palacın, Towards high energy density sodium ion batteries through electrolyte optimization, Energy Environ. Sci. 6 (2013) 2361–2369.
[48] K.C. Klavetter, S. Garcia, N. Dahal, J.L. Snider, J.P. de Souza, T.H. Cell, M.A. Cassara, A. Heller, S.M. Humphrey, C.B. Mullins, Li- and Na-reduction products of meso-Co_3O_4 form high-rate, stably cycling battery anode materials, J. Mater. Chem. A 2 (2014) 14209–14221.
[49] C.H. Wang, C.H. Yang, J.K. Chang, Suitability of ionic liquid electrolytes for room-temperature sodium-ion battery applications, Chem. Commun. 52 (2016) 10890–10893.
[50] E. Markevich, G. Salitra, A. Rosenman, Y. Talyosef, F. Chesneau, D. Aurbach, The effect of a solid electrolyte interphase on the mechanism of operation of lithium–sulfur batteries, J. Mater. Chem. A 3 (2015) 19873–19883.
[51] A. Budi, A. Basile, G. Opletal, A.F. Hollenkamp, A.S. Best, R.J. Rees, A.I. Bhatt, A.P. O'Mullane, S.P. Russo, Study of the initial stage of solid electrolyte interphase formation upon chemical reaction of lithium metal and N-methyl-N-propyl-pyrrolidinium-bis(fluorosulfonyl)imide, J. Phys. Chem. C 116 (2012) 19789–19797.
[52] I.A. Shkrob, T.W. Marin, Y. Zhu, D.P. Abraham, Why bis(fluorosulfonyl)imide is a "magic anion" for electrochemistry, J. Phys. Chem. C 118 (2014) 19661–19671.
[53] W. Luo, C. Bommier, Z. Jian, X. Li, R. Carter, S. Vail, Y. Lu, J.J. Lee, X. Ji, Low-surface-area hard carbon anode for Na-ion batteries via graphene oxide as a dehydration agent, ACS Appl. Mater. Interfaces 7 (2015) 2626–2631.
[54] M. Dahbi, T. Nakano, N. Yabuuchi, T. Ishikawa, K. Kubota, M. Fukunishi, S. Shibahara, J.Y. Son, Y.T. Cui, H. Oji, S. Komaba, Sodium carboxymethyl cellulose as a potential binder for hard-carbon negative electrodes in sodium-ion batteries, Electrochem. Commun. 44 (2014) 66–69.
[55] S. Komaba, T. Ishikawa, N. Yabuchi, W. Murata, A. Ito, Y. Ohsawa, Fluorinated ethylene carbonate as electrolyte additive for rechargeable Na batteries, ACS Appl. Mater. Interfaces 3 (2011) 4165–4168.
[56] Y.H. Zheng, Y.S. Wang, Y.X. Lu, Y.S. Hu, J. Li, A high-performance sodium-ion battery enhanced by macadamia shell derived hard carbon anode, Nano Energy 39 (2017) 489–498.
[57] M. He, K.C. Lau, X. Ren, N. Xiao, W.D. McCulloch, L.A. Curtiss, Y. Wu, Concentrated electrolyte for the sodium-oxygen battery: solvation structure and improved cycle life, Angew. Chem. Int. Ed. 55 (2016) 15310–15314.
[58] X. Fan, L. Chen, X. Ji, T. Deng, S. Hou, J. Chen, J. Zheng, F. Wang, J. Jiang, K. Xu, C. Wang, Highly fluorinated interphases enable high-voltage Li-metal batteries, Chem 4 (2018) 174–185.
[59] J. Wang, Y. Yamada, K. Sodeyama, E. Watanabe, K. Takada, Y. Tateyama, A. Yamada, Fire-extinguishing organic electrolytes for safe batteries, Nat. Energy 3 (2018) 22–29.
[60] M. Dahbi, T. Nakana, N. Yabuuchi, S. Fujimura, K. Chihara, K. Kubota, J.Y. Son, Y.T. Cui, H. Oji, S. Komaba, Effects of hexafluorophosphate and fluoroethylene carbonate on electrochemical performance and the surface layer of hard carbon for sodium-ion batteries, ChemElectroChem 3 (2016) 1856–1867.
[61] C.Y. Li, J. Patra, C.H. Yang, C.M. Tseng, S.B. Majumder, Q.F. Dong, J.K. Chang, Electrolyte optimization for enhancing electrochemical performance of antimony sulfide/graphene anodes for sodium-ion batteries– carbonate-based and ionic liquid electrolytes, ACS Sustain. Chem. Eng. 5 (2017) 8269–8276.
[62] H.C. Chen, J. Patra, S.W. Lee, C.J. Tseng, T.Y. Wu, M.H. Lin, J.K. Chang, Electrochemical Na^+ storage properties of SnO_2/graphene anodes in carbonate-based and ionic liquid electrolytes, J. Mater. Chem. A 5 (2017) 13776–13784.
[63] A. Ponrouch, A.R. Goni, M.R. Polacin, High capacity hard carbon anodes for sodium ion batteries in additive free electrolyte, Electrochem. Commun. 27 (2013) 85–88.

Electronic Supplementary Information for

Moderately Concentrated Electrolyte Improves Solid–Electrolyte Interphase and Sodium Storage Performance of Hard Carbon

Table S1. First-cycle CE values, capacities (mAh g^{-1}), and rate capabilities of HC electrodes measured in various electrolytes.

	1 mol dm^{-3} $NaClO_4$ DEC:EC	1 mol dm^{-3} $NaPF_6$ PC:EC	1 mol dm^{-3} NaFSI DEC:EC	1 mol dm^{-3} NaFSI PC	1 mol dm^{-3} NaFSI PC:EC
First-cycle CE	57 %	59 %	61 %	62 %	64%
0.03 A g^{-1}	205	214	191	210	218
0.05 A g^{-1}	187	193	156	185	194
0.1 A g^{-1}	138	143	107	136	145
0.5 A g^{-1}	89	92	72	87	93
0.7 A/g^{-1}	81	82	68	78	84
1 A g^{-1}	72	74	62	66	75
Rate capability $C_{1\ A}/\ C_{0.03\ A}$	35.1%	34.5%	32.4%	31.4%	34.4%

Table S2. First-cycle CE values, capacities (mAh g^{-1}), and rate capabilities of HC electrodes measured in various NaFSI electrolytes.

	NaFSI/PC			NaFSI/PC:EC		
	1 mol dm^{-3}	2 mol dm^{-3}	3 mol dm^{-3}	1 mol dm^{-3}	2 mol dm^{-3}	3 mol dm^{-3}
First-cycle CE	62%	69%	75%	64%	71%	85%
0.03 A g^{-1}	210	228	237	218	235	253
0.05 A g^{-1}	185	206	219	195	219	238
0.1 A g^{-1}	136	152	163	145	166	185
0.5 A g^{-1}	87	100	109	93	114	133
0.7 A/g^{-1}	78	89	100	84	105	124
1 A g^{-1}	66	78	86	75	92	114
Rate capability $C_{1\ A}/\ C_{0.03\ A}$	31.4%	34.2%	36.2%	34.4%	39.1%	45.0%

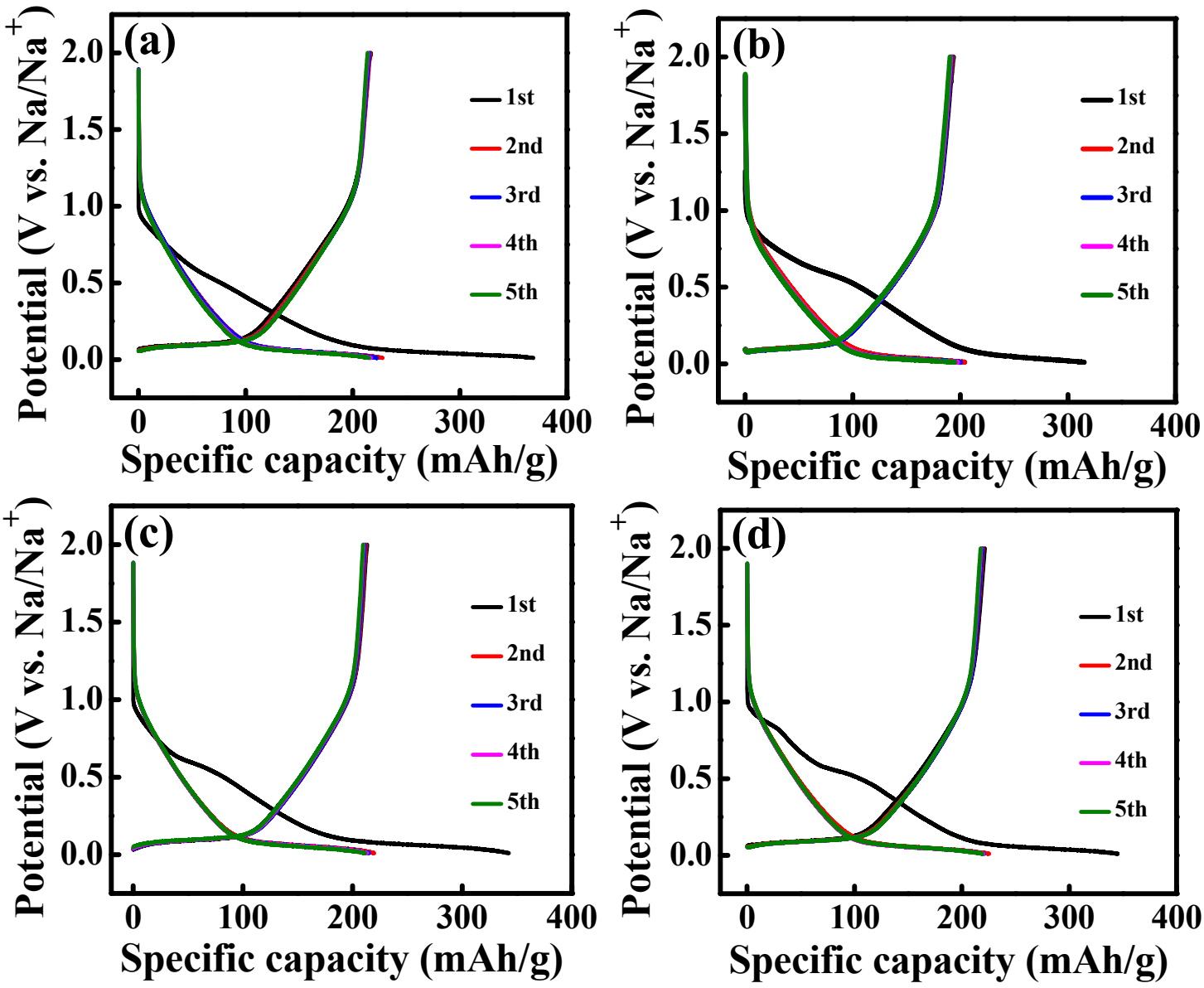

Figure S1. Initial five charge–discharge curves of HC electrodes measured in (a) 1 mol dm^{-3} $NaPF_6$/PC:EC, (b) 1 mol dm^{-3} NaFSI/DEC:EC, (c) 1 mol dm^{-3} NaFSI/PC, and (d) 1 mol dm^{-3} NaFSI/PC:EC electrolytes.

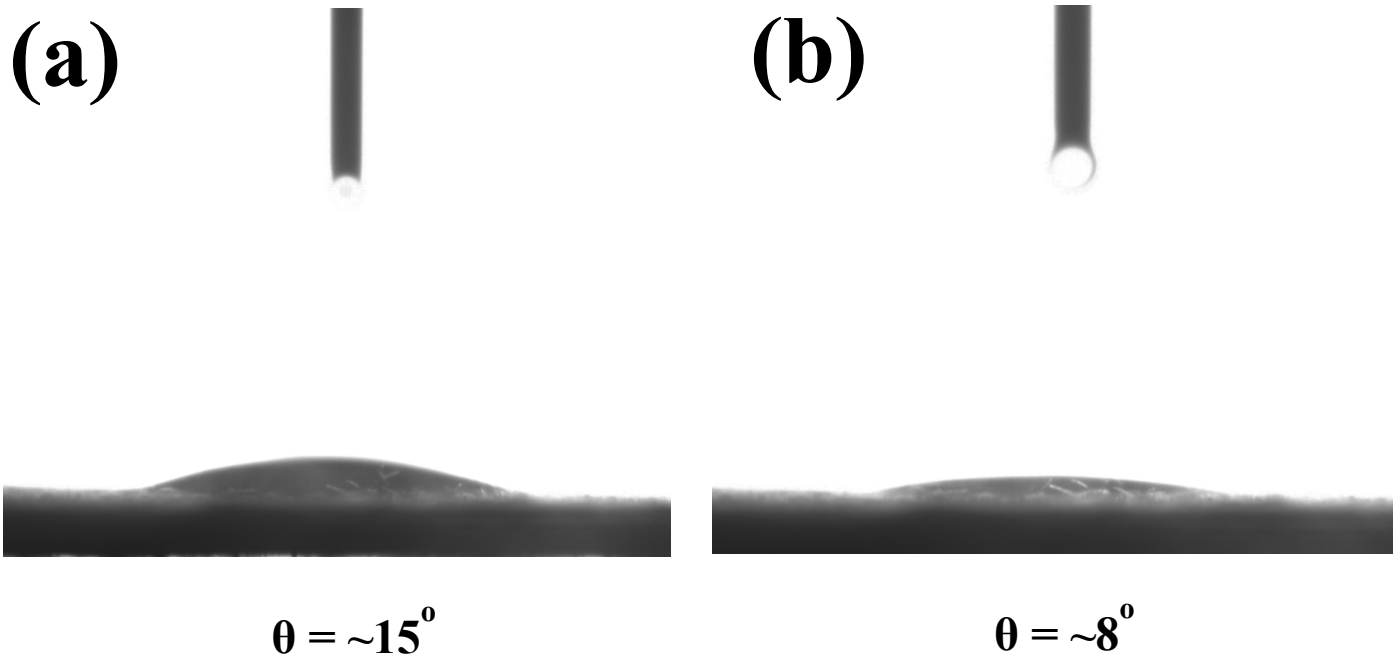

Figure S2. Contact angle measurements of 3 mol dm^{-3} NaFSI/PC:EC electrolyte with the (a) HC electrode and (b) separator.

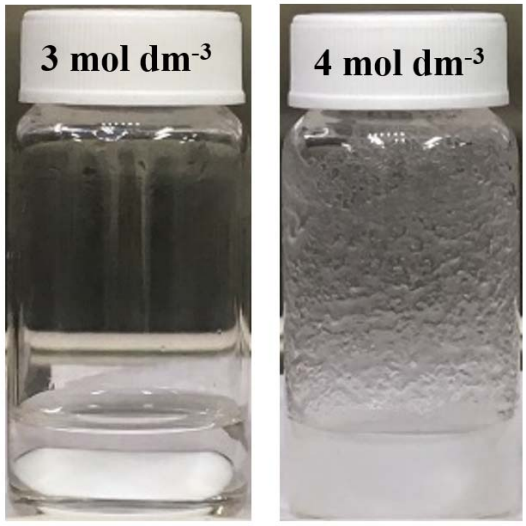

Figure S3. Images of 3 and 4 mol dm^{-3} NaFSI/PC:EC electrolytes.

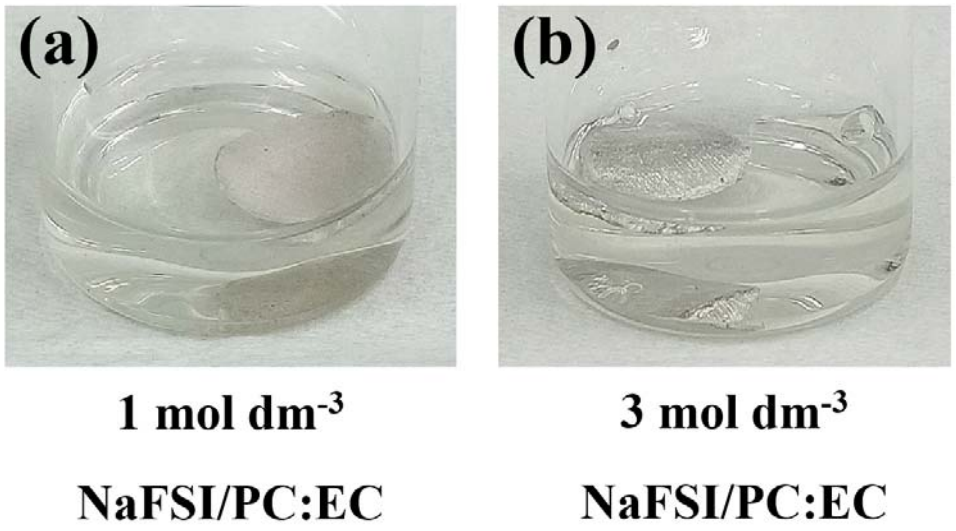

Figure S4. Images of Na foil immersed in (a) 1 mol dm^{-3} and (b) 3 mol dm^{-3} NaFSI/PC:EC electrolytes after 5 days.

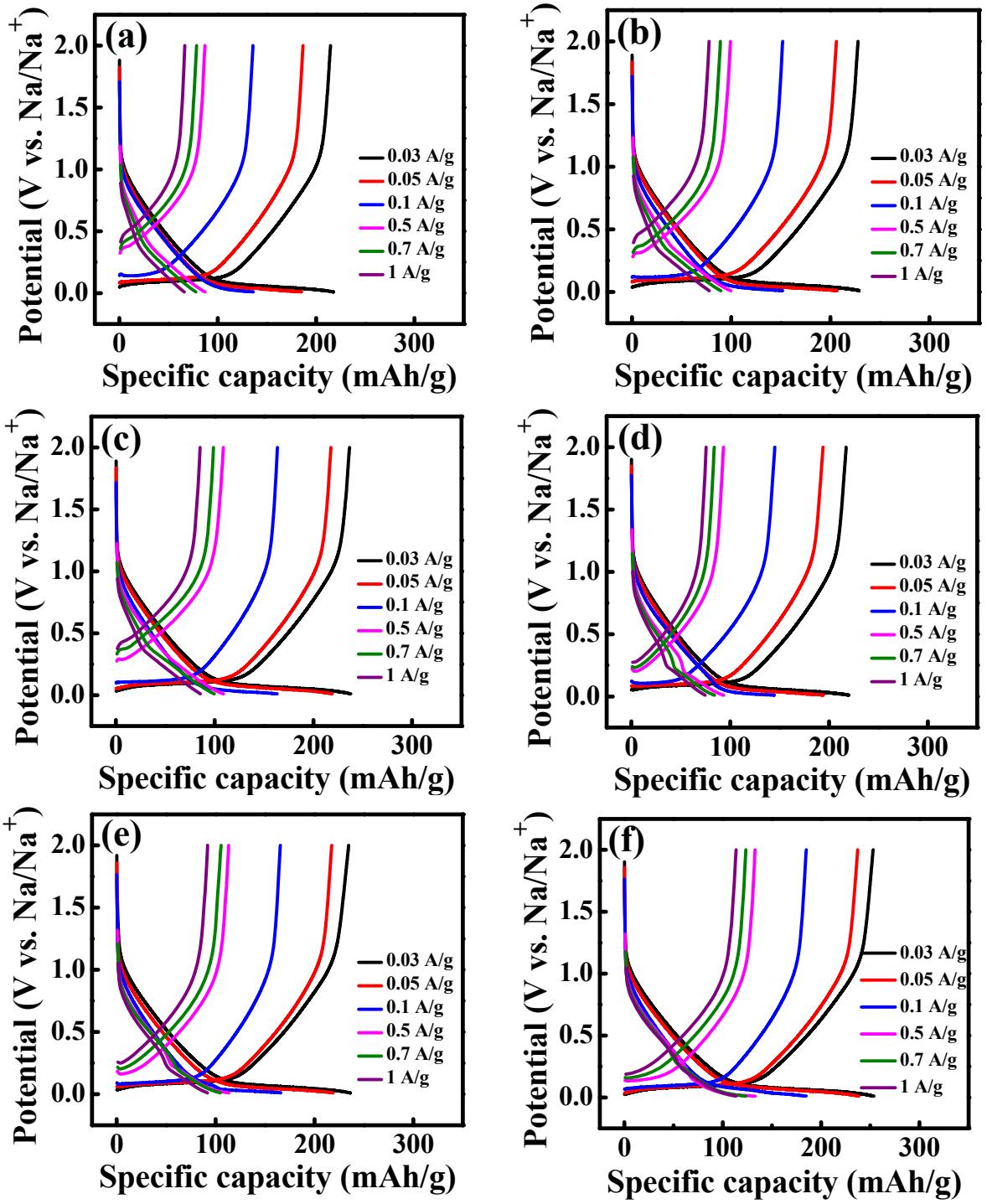

Figure S5. Charge–discharge curves of HC electrodes measured in (a) 1 mol dm^{-3}, (b) 2 mol dm^{-3}, (c) 3 mol dm^{-3} NaFSI/PC, and (d) 1 mol dm^{-3}, (e) 2 mol dm^{-3}, (f) 3 mol dm^{-3} NaFSI/PC:EC electrolytes with various rates.

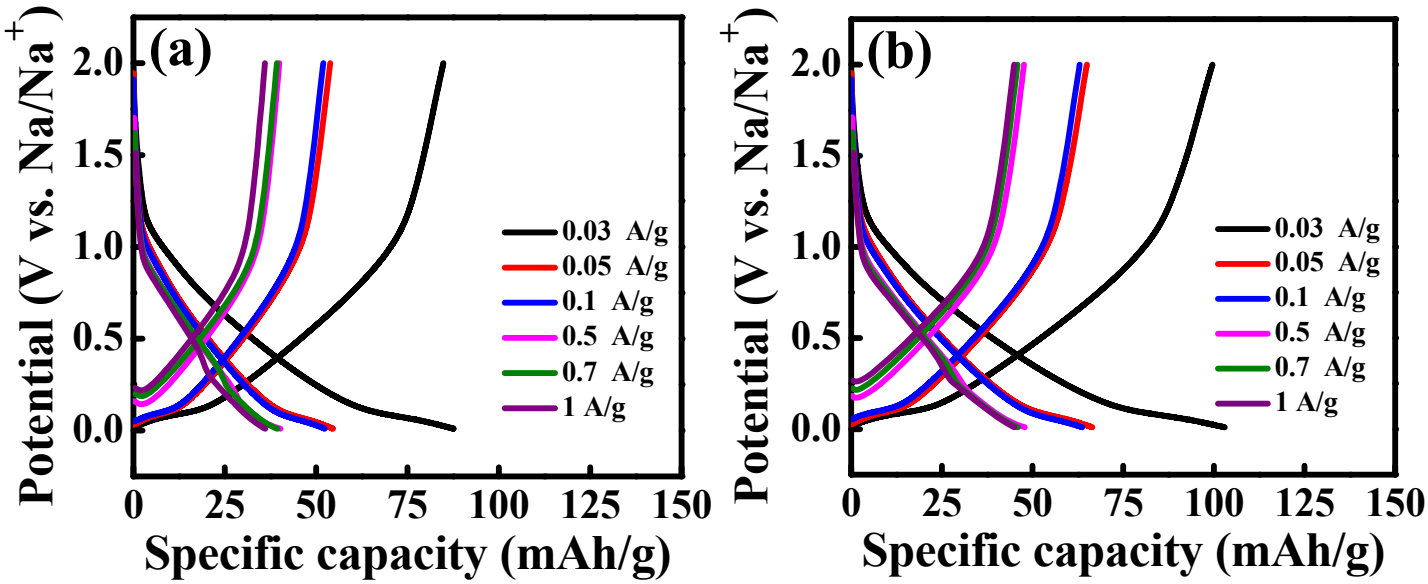

	1 mol dm^{-3} NaFSI PC:EC	3 mol dm^{-3} NaFSI PC:EC
0.03 A g^{-1}	85 mAh g^{-1}	100 mAh g^{-1}
0.05 A g^{-1}	54 mAh g^{-1}	65 mAh g^{-1}
0.1 A g^{-1}	52 mAh g^{-1}	63 mAh g^{-1}
0.5 A g^{-1}	40 mAh g^{-1}	48 mAh g^{-1}
0.7 A/g^{-1}	39 mAh g^{-1}	46 mAh g^{-1}
1 A g^{-1}	36 mAh g^{-1}	45 mAh g^{-1}
Rate capability $C_{1\ A}/\ C_{0.03\ A}$	42.3%	45.0%

Figure S6. Charge–discharge curves of carbon black electrodes measured in (a) 1 mol dm^{-3} and (b) 3 mol dm^{-3} NaFSI/PC:EC electrolytes with various rates.

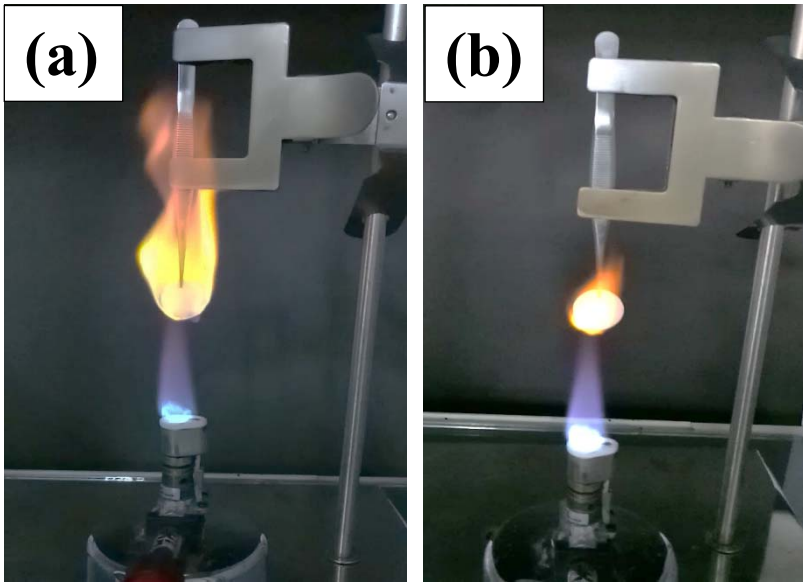

Figure S7. Flammability tests (a) 1 mol dm^{-3} $NaPF_6$/PC:EC and (b) 3 mol dm^{-3} NaFSI/PC:EC electrolytes.

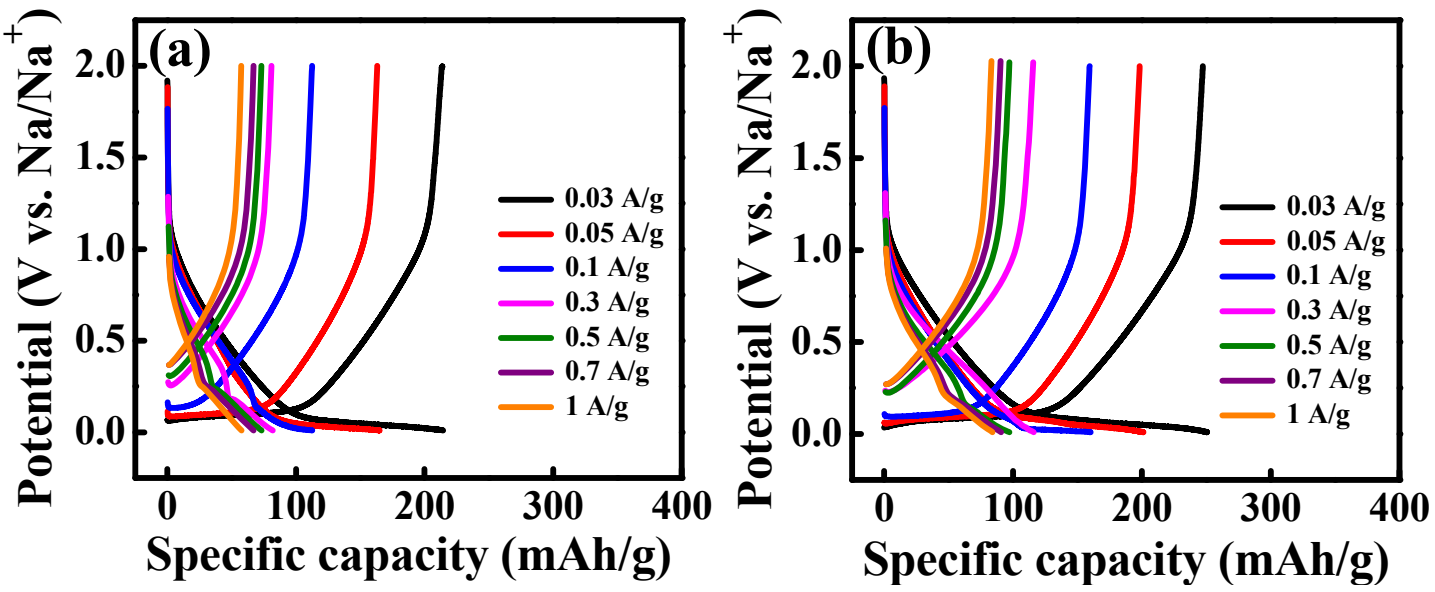

	1 mol dm^{-3} NaFSI PC:EC	3 mol dm^{-3} NaFSI PC:EC
0.03 A g^{-1}	214 mAh g^{-1}	247 mAh g^{-1}
0.05 A g^{-1}	163 mAh g^{-1}	198 mAh g^{-1}
0.1 A g^{-1}	113 mAh g^{-1}	159 mAh g^{-1}
0.3 A g^{-1}	81 mAh g^{-1}	116 mAh g^{-1}
0.5 A/g^{-1}	73 mAh g^{-1}	97 mAh g^{-1}
0.7 A/g^{-1}	68 mAh g^{-1}	90 mAh g^{-1}
1 A g^{-1}	58 mAh g^{-1}	83 mAh g^{-1}
Rate capability $C_{1\ A}/\ C_{0.03\ A}$	27.1%	33.6%

Figure S8. Charge–discharge curves of thick HC electrodes (with a loading amount of 11.5 mg cm^{-2}) measured in (a) 1 mol dm^{-3} and (b) 3 mol dm^{-3} NaFSI/PC:EC electrolytes with various rates.